Lab on a Chip

Cite this: *Lab Chip*, 2012, **12**, 3190–3196

www.rsc.org/loc

PAPER

Real-time monitoring of strand-displacement DNA amplification by a contactless electrochemical microsystem using interdigitated electrodes†

Xinxin Fang,[ab] Huanqian Zhang,[a] Feng Zhang,[ab] Fengxiang Jing,[a] Hongju Mao,[a] Qinghui Jin*[a] and Jianlong Zhao*[a]

Received 20th April 2012, Accepted 22nd May 2012
DOI: 10.1039/c2lc40384f

This paper reports the design and implementation of a contactless conductivity detection system which combines a thermal control cell, a data processing system and an electrochemical (EC) cell for label-free isothermal nucleic acid amplification and real-time monitoring. The EC cell consists of a microchamber and interdigitated electrodes as the contactless conductivity biosensor with a cover slip as insulation. In our work, contactless EC measurements, the effects of trehalose on amplification, and chip surface treatment are investigated. With the superior performance of the biosensor, the device can detect the amount of pure DNA at concentrations less than 0.1 pg μl^{-1}. The EC cell, integrated with a heater and a temperature sensor, has successfully implemented nicking-based strand-displacement amplification at an initial concentration of 2.5 μM and the yields are monitored directly (dismissing the use of probes or labels) on-line. This contactless detector carries important advantages: high anti-interference capability, long detector life, high reusability and low cost. In addition, the small size, low power consumption and portability of the detection cell give the system the potential to be highly integrated for use in field service and point of care applications.

Introduction

With the rise of the concept of lab-on-chip (LOC), the analysis of DNA based on microchips has sparked great interest in the fields of molecular biology and biotechnology. Usually, the amount of DNA in the samples is not sufficient for detection. Therefore it is necessary to amplify the nucleic acid to reach the detection limit before analysis. The most common way to achieve this is through PCR amplification. There are two ways to perform PCR. One is time-domain, in which a reservoir or pool allows temperature changing with PCR cycling. The other way is space-domain, which executes PCR cycles by moving the reaction mixture between different temperatures zones. In addition to PCR, which is based on thermal cycling, a variety of isothermal amplification methods have been developed, including rolling circle amplification, loop-mediated isothermal amplification (LAMP), and strand-displacement amplification (SDA). For applications that require more simple instruments, isothermal DNA chips are much easier to integrate than PCR chips.

Fluorescence detection (FD) is the traditional way to detect DNA products. FD demands fluorescent labeling and an expensive optical detection system that is difficult to miniaturize and is only adopted in laboratories. Besides, FD has the disadvantage of high background interference. On the other hand, electrochemical (EC) DNA analysis displays rapid, sensitive, simple, non-toxic, low-cost and effective merits compared to the shortcomings of FD. In the literature,[1] the application of EC technology in PCR amplification has been reviewed comprehensively. In addition, a few literature reports have reported micro-devices that integrate PCR amplification with EC detection. According to the reports, LAMP products and SDA products are also detected successfully using EC methods.[2,3]

EC DNA detection is divided into a direct way and an indirect way. The former is based on direct electron transfer on the electrode surface, and some components of DNA in a certain potential window have potential EC activity. For example, Ozkan and co-workers[4] detected PCR amplicons using the intrinsic guanine signal. In the indirect detection method, electron transfer is implemented and detected by adding redox indicators which selectively bind to and hybridize with DNA (such as methylene blue,[5–7] Hoechst 33258,[8,9] daunomycin,[10] Os[(bpy)^{2}DPPZ]$^{2+}$,[11] and echinomycin[12]). Some researchers have reported that gold particles used for detecting DNA hybridization not only have good biocompatibility, but also their surface catalyzes the deposition of silver particles, thereby increasing the signal to noise ratio.[13–15] In recent years, EC detection has been widely developed and has reached a high sensitivity (at least ng μl^{-1} level). Indeed, hybridization using labeled single-stranded

[a]*State Key Laboratory of Transducer Technology, Shanghai Institute of Microsystem and Information TechnologyChinese Academy of Science, China. E-mail: jinqh@mail.sim.ac.cn; jlzhao@mail.sim.ac.cn; Fax: +86 21 62511070-8714; Fax: +86 21 62511070-8714; Tel: +86 21 62511070-8703 Tel: +86 21 62511070-5801*
[b]*Graduate School of the Chinese Academy of Science, China*
† Electronic Supplementary Information (ESI) available. See DOI: 10.1039/c2lc40384f

(ss) DNA probes in the EC method has even allowed single molecule detection.[16] However, using probes increases the difficulty of the technique and is not recommended for use when measuring raw or highly impure samples. It must also be considered that when DNA complexes with redox indicators, the spatial structure of DNA changes may affect the continuous binding efficiency, which is likely to weaken the sensitivity.

According to the previous study, the electrodes used for DNA detection all work by contacting the target sample, whether by a labeled or label-free approach. The contact detection principle is based on current or impedance changes on the electrode surface caused by the accumulation of the target or complex. In order to remove undesirable residues on the electrode surface from previous measurements, the electrodes have to be regenerated every time prior to the detection. The regeneration step makes the operation more complicated and is likely to impact on the performance of the next detection using the same electrodes. The electrode surface is easily saturated and fouled, causing low reproducibility, short lifetime, and limited detection range. Although disposable electrodes may be a solution, they are costly and inconvenient. Moreover, the voltage applied to the solution could result in hydrolysis, which is not good for achieving sensitive detection.

To overcome these limitations, this paper proposes a novel contactless EC means for real-time monitoring of isothermal nucleic acid amplification. The system is based on capacitive-coupling with an insulating layer located between the electrodes and the solution. Because the electrodes are not in contact with the solution, the background noise is reduced greatly and the contactless mode achieves low detection limits.[17] In addition, there is no problem of bubble formation at the electrode surface caused by direct contact. In this work, non-contact interdigitated electrodes (IDEs) in place of traditional single-finger electrodes as the biosensor achieve great sensitivity (0.1 pg μl^{-1}) and great resolution. The device is easily integrated, simple to operate, highly resistant to contamination and highly reusable, and the detection efficiency is superior to traditional single-finger electrode detectors. We have successfully implemented isothermal nicking-dependent strand-displacement amplification (NSDA) on the microchip, dismissing the use of labels or probes, and have detected the products in real time within several minutes. By using this system, we explore the roles of trehalose and pretreatment of the chamber in the reaction, and improve the performance of NSDA.

Experimental

Working principle

In most EC biochips, PCR is a widespread means by which to amplify target DNA. Nevertheless, PCR has its limitations when applied to micro-systems. Especially, it should be noted that PCR, which is based on thermal cycling, demands accurate temperature control and needs extra cooling devices in order to produce effective results. It is difficult to integrate all of the components at the micro-scale, and this limits the application. To fix this problem, our study used the isothermal NSDA as a substitute for PCR amplification. NSDA was initially investigated by Walter *et al.*.[18] Recently, Joneja *et al.*[19] demonstrated linear amplification of long DNA molecules by NSDA with the help of several newly engineered and commercially available nicking endonucleases. The basic principle of NSDA is illustrated in Fig. 1. The single-stranded template hybridises with primers before a nicking endonuclease cleaves the target DNA in the recognition site. Then the nicking site is extended under the control of a DNA polymerase and displaces the original DNA strand. At the same time, the recognition site is regenerated. The extension continues until the nicking meets the end point. The products are treated as new templates for repeated nicking and strand displacement, resulting in exponential amplification. The template we used here does not require denaturation or any pretreatment prior to measurement, and is amplified exponentially. The number of products increases along with the increase in the cycle number, thereby strengthening the conductivity of the reaction solution.[20] Consequently, the capacitance change is sensed by the IDE sensor.

So far, most contactless studies have been adopted in electrophoresis chips, mainly detecting ions and amino acids.[21,22] A few groups of researchers demonstrated DNA analysis by the use of the IDE approach, employing DNA hybridization or impedance spectroscopy.[23,24] Nevertheless, there are few reports on the real-time monitoring of DNA amplification by the approach of the contactless IDEs. In the present study, we aim to combine isothermal DNA amplification with on-line real-time direct determination by means of contactless IDEs for the first time, dispensing with the use of probe immobilization or impedance spectroscopy scanning.

The simplest equivalent circuit of the capacitive coupling, contactless conductivity detector (C^4D) microchip sensor[25] is illustrated in Fig. 2 (only the fundamental elements are included). A very thin insulating layer not only isolates the electrodes from the solution, but also allows them to be very close together without actually contacting each other. The capacitance between the electrodes and the solution is described as follows:

$$C_w = \frac{\varepsilon_r \varepsilon_0 ax}{d} \quad (1)$$

where C_w and ε_r represent the capacitance and the dielectric constant of the dielectric layer, respectively; d is the thickness of the layer; ε_0 is the dielectric constant of air; and ax is the working area of the electrodes. Larger values of C_w correspond to a more sensitive detector. Thus, with an increase of the working area of

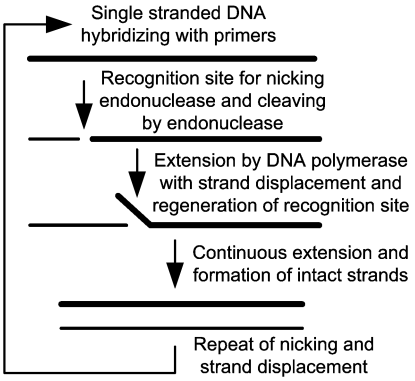

Fig. 1 Principle stages involved in isothermal nicking-dependent strand-displacement amplification (NSDA) reaction.

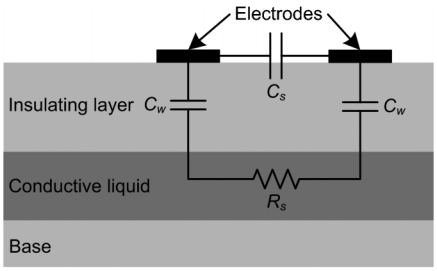

Fig. 2 The simplified equivalent circuit model for the C^{4}D microchip sensor. C_w, R_s, and C_s stand for the wall capacitance, the cell resistance, and the total stray capacitance between the two electrodes, respectively.

the electrodes and a decrease of the insulation thickness, the detector becomes more sensitive. At appropriate C_w values, the small changes in the solution lead to detectable changes, as confirmed by the readout of the sensor, which are measured using precise equipment. Capacitive coupling electrodes have to work at AC excitations. As reported, the C^{4}D has achieved an average detection limit of 0.4 μM inorganic ionic detection by using a sine wave excitation with a frequency of 50 kHz and peak-to-peak voltage ($V_{p\text{-}p}$) of 20 V.[26]

EC electrodes have different kinds of structure such as single-finger electrodes and IDEs. There is only one finger working as a sensing finger for the former electrode type, whose properties are relatively simple and have been researched a great deal. Meanwhile, IDEs are of a comb-like geometry (Fig. 3C), of which a number of fingers contribute to sensing, and that is the reason why the IDEs get higher sensitivity in contrast to the single-finger electrodes. Because the structure of the IDEs is diversified, as well as each finger influencing its neighbors when working at high frequencies, the characteristics of the IDEs are

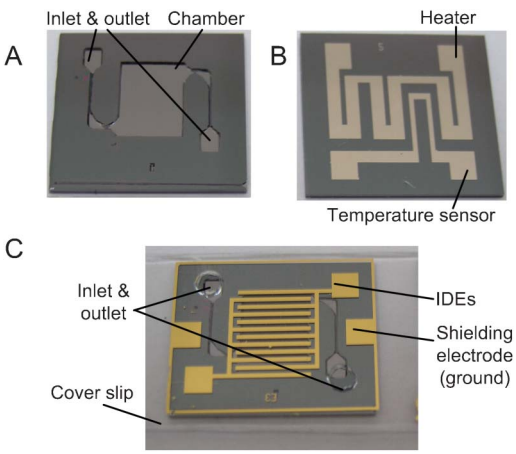

Fig. 3 Photographs of the microchips. (A) is the top view of the silicon wafer substrate with an etched chamber for NSDA and (B) shows the bottom view of the silicon substrate integrated with a heater (Pt) and a temperature sensor (Pt). The chamber is of 50 mm^2 area and 150 μm depth. The fluidic channels are 50 μm wide. Both the resistance of the heater and the sensor is about 45 Ω. (C) is the fabricated micro-system integrating the silicon substrate with the IDEs (using a cover slip as insulation). The diameter of the holes, the width of interdigitated fingers, the distance between the adjacent fingers and the length of the fingers are 2 mm, 0.3 mm, 0.3 mm, and 6 mm, respectively. The size of the integrated chip is 1.5 cm × 1.2 cm.

more complex and harder to define. The output strength of the IDEs changes with respect to several factors, including the working area of the electrodes, the number, the width and the length of the fingers, and the spacing between them.[27] For example, the impedance of each electrode increases if the number of fingers is too small, while the stray capacitive noise dominates if the number of electrode fingers is excessive. In both cases, the sensitivity toward the target impedance is decreased. For this reason, a tradeoff between the impedance and the detection accuracy of the sensor should be made considering the application requirements.

Chip design and fabrication

In previous literature of C^{4}D, the reports mainly employ polydimethylsiloxane (PDMS),[26,28] methyl methacrylate (PMMA)[29] and glass substrates[30,31] as insulation. By controlling the excitation conditions, the contactless sensors have achieved good sensitivity. The contactless electrodes induce stronger differential signals with increasing the insulating dielectric constant, as well as decreasing of the insulating thickness. PDMS is widely used as insulation because of its simple manufacture and low cost. However, the dielectric permittivity of PDMS is not as good as that of glass. Furthermore, glass is less likely to adsorb contaminants on the surface when compared with PDMS and is simple to fabricate. Cover slips of 100 μm thickness have been demonstrated to perform well in contactless electrophoresis devices.[31] Here, we propose common commercial cover slips to act as the insulation as well as the substrate for the IDEs.

The microchip we designed consists of two substrate layers. The top layer is a cover slip with gold IDEs printed on the top side and two punched holes as inlet and outlet respectively (Fig. 3C). The bottom layer is a silicon wafer substrate with a chamber (Fig. 3A) etched on the top side, as well as a platinum (Pt) temperature sensor and a Pt heater (Fig. 3B) integrated on the bottom side. The chamber was bonded with the bottom of the cover slip using UV-glue (Fig. 3C).

For the chamber layer, the following fabrication techniques were employed (Fig. 4A): first, the mask was patterned on a double-sided polished and oxidized silicon wafer substrate using AZ4620 photoresist; second, HF was used to etch the exposed silicon dioxide; after the photoresist was dissolved away using acetone, 50% KOH is used to etch the silicon in a 60 °C water-bath. Both gold electrodes and Pt electrodes were fabricated by the standard lift-off process (Fig. 4B): first, the substrates were patterned using the AZ4620 photoresist; then the substrates were coated with Ti as an adhesion layer followed by the desired metal (Au for the IDEs and Pt for the temperature sensors and heaters); finally the photoresist was dissolved by immersing the substrates in acetone and the metal electrodes not coated with photoresist remained on the substrate; lastly, holes in the cover slips were drilled for use as the inlet and outlet.

Reagents and sample preparation

The volume consumption in one chip was approximately 7.5 μl. Every 20 μl of NSDA mixture contained 2 μl of NEBuffer 3, 1 μl of bovine serum albumin (BSA, 0.05%), 1 μl of dNTP, 2 μl of F1/F2 primers (0.5 μM/5 μM), 2 μl of R1/R2 primers (0.5 μM/

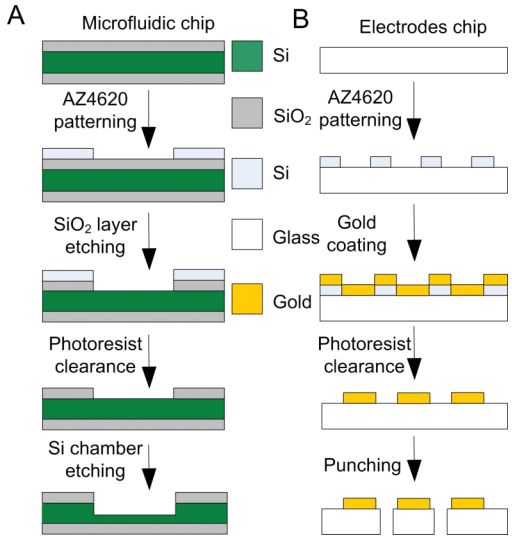

Fig. 4 Process schemes of the microchip. (A) shows the wet etching of microchamber in a silicon substrate. (B) is the lift-off process for formation of metal electrodes.

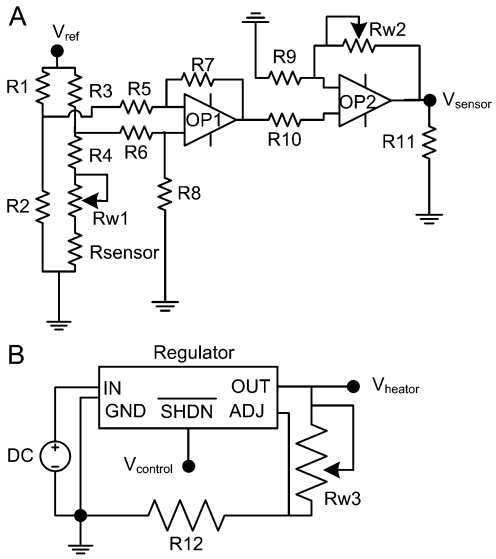

Fig. 5 Circuit schemes of thermal control. (A) shows the circuit for converting temperature signals to the readout voltage, where R_{sensor} is the resistance of the sensor. The magnification of the output V_{sensor} is adjusted according to R_{w2}. (B) shows the regulation of the voltage of the heater, where V_{heater} is the output voltage and R_{w3} is used to modulate the amplitude of V_{heater}. Both the V_{sensor} port in (A) and the $V_{Control}$ port in (B) are connected to a DAQ device.

5 μM), 0.5 μl of Nb.BsmI (10 U μl^{-1}), 0.25 μl of Bst DNA polymerase (8 U μl^{-1}), 1 μl of ssDNA templates (2.5 μM) and 10.25 μl of ultra-pure water. BSA was obtained from Sigma-Aldrich (Germany) and was diluted by 1 × PBS solution. Both the Bst DNA polymerase and the nicking endonuclease Nb.BsmI (including NEBuffer 3) were purchased from New England BioLabs (NEB, USA). Nucleotides were acquired from GE (USA). Short ssDNA templates of specific sequences and primers (see ESI†) were synthesized by TaKaRa Biotechnology (Dalian, China). DNA templates (2.5 μM) were linked from two short ssDNA chains using T4 DNA ligase (NEB) before isothermal amplification. A lab water purification system from Millipore SAS (France) was used to supply ultra-pure water. To observe the effect of nicking enzymatic activity, 2 M of D-(+)-trehalose (Shanghaikayon Biological Technology, China) solution replaced part of the water in the NSDA mixture.

Though the yields of NSDA were detected using an EC model, it is still necessary to confirm the results by gel electrophoresis using 2% of Biowest agarose gel (Gene Company, Hong Kong) and visualizing it with a UV camera (Bio-Rad Gel Doc XR+, Bio-Rad Laboratories, USA). The 100 bp DNA Ladder Marker was provided by TaKaRa (Japan), and a double-stranded DNA aqueous solution was purified from the DNA Ladder Marker using the protocol and reagents from the QIAquick PCR purification Kit (QIAGEN, Germany).

Instrumentation and measurement

Aiming to functionalize the temperature sensor and the heater, the thermal control circuits (Fig. 5) and software were designed and built. The correlation between the resistance and the temperature of the sensor is as follows:[32]

$$R_T = R_0(1 + \alpha(T_s - T_0)) \quad (2)$$

where R_T and R_0 represent the resistances of the sensor at temperatures T and T_0 (reference temperature), respectively, and α is the temperature coefficient of resistance (TCR). The temperature is converted to a voltage using a Wheatstone bridge (Fig. 5A). The resistance changes with temperature variation and the differential voltage varies according to the following:

$$\Delta V = \frac{1}{4}\frac{\Delta R}{R_1} V_{ref} A T \quad (3)$$

Following the conditioning and magnifying process, the differential voltage provides feedback information for a control program (Labview, NI, USA) through a data acquisition (DAQ) card (USB2811, Art Technology, China). The voltage loaded on the heater is adjusted by means of a voltage regulator (Fig. 5B), which is commanded by employing a pulse-width modulation (PWM) algorithm. With the precise calibration and proper PWM control, the temperature of the microchip achieved 65 °C within 10 s starting from room temperature, and maintained a stable temperature with a precision of ±0.2 °C. In addition, the current of the IDEs was transformed to voltage signals using an operational amplifier with a feedback resistor of 1 MΩ, and then was acquired by DAQ.

We employed an Agilent voltage source module known to generate several AC waveforms of frequencies from 1 HZ to 1 MHz and $V_{p\text{-}p}$ from 0 V to 10 V as the excitation. The DAQ card possesses a high sampling frequency up to 500 kHz, a sampling $V_{p\text{-}p}$ range from −10 V to 10 V, and an accuracy of 16 bits. The microchip module and the circuits were all shielded effectively from external signal interference and background noise by placing them in a Faraday cage with the shell connected to the ground. On the PC terminal, the control program performed data filtering, temperature control, display and saving of the results.

Before the reaction test, the micro-chamber was permeated with 0.5% BSA for about 30 min to get rid of enzyme adsorption to the wall. Then, the BSA was washed away and 7.5 μl of the sample was injected by vacuum pumping, followed by sealing the inlet and the outlet with mineral oil. The amplification at 65 °C and EC measurement were executed concurrently. The baseline was subtracted from the readout to correct for the background, followed by filtering and smoothing. After each measurement, the chip was rinsed with large quantities of washing buffer (including Tween and PBS) and water.

Results and discussion

To find the optimized conditions of the detector, the response to different AC excitation was observed. The response was found to be a positive correlation to the $V_{p\text{-}p}$ and a certain range of the frequency. It should be mentioned that as the frequency increased above 45 kHz, the attenuation of the operational amplifiers in the circuits became more evident and the output waveform was distorted to some degree. Meanwhile, the noise was intensified with increased frequency, leading to more severe interference. Moreover, it was observed that the output peak-peak values were more unstable when the exciting frequency happened to be a multiple of 10 kHz. Though the mechanism still stayed unclear, it may be related to the performance of the PCB circuits. To sum up, a frequency of 35 kHz was adopted.

Before the reaction measurements, a simplified model without thermal control units was designed to validate the feasibility of this method. A volume of 7.5 μl DNA aqueous solution was sufficient to determine the difference, as shown in Fig. 6. Notably, the differential potential is positively proportional to the logarithm of the DNA concentration. The results indicate that the detector has a detection limit of 0.1 pg μl^{-1}, and distinguishes from 0.1 pg μl^{-1} to 0.5 pg μl^{-1}. Besides, when the sample concentrations are higher than 1 ng μl^{-1}, a maximum conductivity is reached and remains constant. The detector is likely saturated at high concentrations and is thus more sensitive to low ionic concentrations. Although the ions in the reaction mixture are more complex than pure DNA solutions, the device is feasible for detection of real-time nucleic acid amplification.

With the optimized conditions of this system, the NSDA reaction was successfully carried out on the microchip containing a template DNA concentration of 2.5 μM. The real-time EC signals of the NSDA reaction free of trehalose were recorded using the designed equipment (Fig. 7). Time points were taken per minute once the temperature had stabilized at 65 °C. The conductivity decreased during the first minute, and then sharply increased during the next 5 min. The differential potential was nearly constant at approximately 90 mV during the first 10 min following a moderate increase. Template DNA, enzymes (Bst polymerase and nicking endonuclease) and nucleotides are attributed to the changes in conductivity. After an initial pre-activation of the polymerase and the endonuclease at 65 °C, enzymes and primers bind to the sites of the DNA templates, reducing the amount of free ions in solution.[20] Consequently, this leads to a decline of the conductivity. Each time the DNA polymerase incorporates a deoxyribonucleoside monophosphate from a corresponding deoxynucleoside triphosphate (dNTP), a single pyrophosphate ion and hydrogen ions are released into solution. The ion production rate increases the solution conductivity. In the early stage of the reaction, the consumption of dNTP and the generation of ions provide a remarkable contribution to the overall conductivity of the mixture. However, as the cycle numbers increase and the yields accumulate, the viscosity of the solution also increases.[20] The viscosity begins to offset the increased impact of ion production, slowing down the rate of EC signal change. Finally, the conductivity variation goes through a maximum constant when the viscosity and ions are almost balanced. It can be seen that the NSDA reaction in this case does not need initial cycles like C_t and easily achieves a detectable level compared with PCR, greatly saving time and cost. This excellent performance is primarily attributed to the efficient amplification of NSDA and the high sensitivity of the IDEs. The qualitative measurement of the real-time isothermal target DNA amplification is quickly and effectively achieved by the contactless sensors.

Compared with the conductivity of the pure DNA ladder solution (Fig. 6), the conductivity variation in Fig. 7 is smaller and is quickly saturated (within 10 min). In addition to the role of the viscosity and the strong ionic background of NSDA, conductivity variation also depends on the performance of the

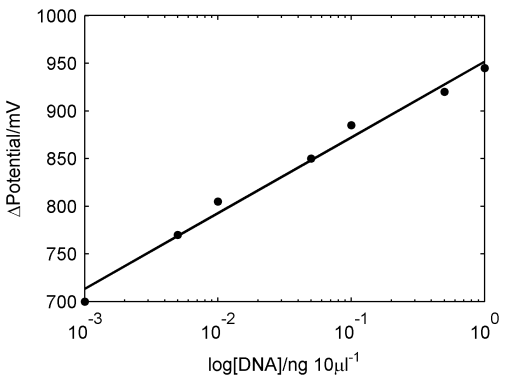

Fig. 6 Calibration plot of the differential potential converted from peak-peak current of the IDEs against the mass of the purified DNA ladder. The measurement was executed at 25 kHz and 10 V. The sample volume is 7.5 μl.

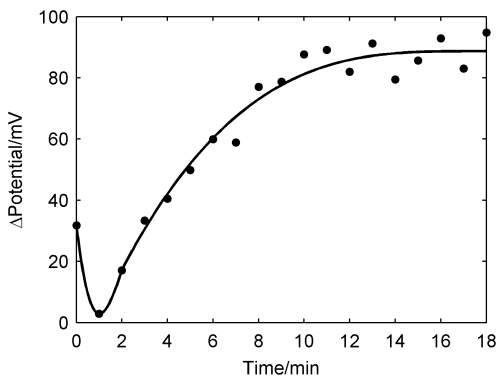

Fig. 7 Voltammograms show the differential voltages during the NSDA reaction free of trehalose. The chamber was incubated with 0.5% BSA for 30 min before the reaction. The measurement was executed at 35 kHz and 10 V.

polymerase and the endonuclease, which are easily deactivated and easily adsorbed to the wall of the microchamber, causing incomplete reaction processing and a slow rate of the conductivity changing. Despite the results in Fig. 7 being clear enough to show the amplification products, there is still a need to improve the conditions for measuring the amplification products at lower template concentrations. A number of studies show that trehalose is not only effective in preserving cells and macromolecules, but also plays a key role in protecting enzymes by remaining active for longer and at higher temperatures. Therefore, 2 M of trehalose was employed to overcome the problem of enzyme activity by replacing part of water in the reaction mixture. The resulting conductivity changes are shown in Fig. 8. After a slight fall in conductivity during the initial few seconds of measurement, the conductivity rose for the next 20 min. The maximum differential potential was observed to increase to 300 mV, which is higher than the results shown in Fig. 7. The data reveals that the ion production dominates the conductivity changes over a longer time and gains a higher signal resolution. With the help of trehalose, the polymerase and the endonuclease have a longer working life and enhanced activity and the execution time is reduced. The expected band between 100 bp and 200 bp is visualized on the agarose gels (Fig. 9). Besides, a small amount of products of less than 100 bp resulted from nonspecific primer-dimer amplification.

In addition to the effects of the trehalose on the reaction enzymes, the pretreatment of the chip with BSA also impacts the amplification efficiency. The BSA-coated mechanism is based on reducing the adsorption of the mixture ingredients to the microchamber wall (in particular the polymerase and the endonuclease), ensuring an adequate amount of reactants and enzymes required for the amplification. Chips were coated with 0.5% of BSA for 60 min before sample injection and measurement. The conductivity variation during amplification against reaction time is shown in Fig. 10. Compared with the reaction carried out on chips incubated with BSA for 30 min (Fig. 8), a maximum differential potential of 500 mV was reached, as shown in Fig. 10. The data indicate that chips coated with BSA result in better amplification efficiency and larger variation in conductivity. However, it is not appropriate to fill the chamber with BSA for too long a time as it may be difficult to rinse away, which could affect the regeneration of the microchips.

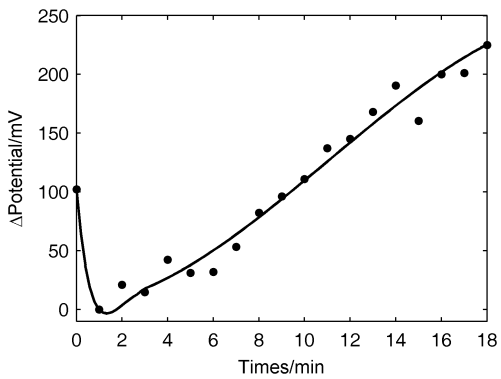

Fig. 8 Voltammograms show the NSDA reaction with 30 mM of trehalose. The chamber was incubated with 0.5% BSA for 30 min before the reaction. The measurement was executed at 35 kHz and 10 V.

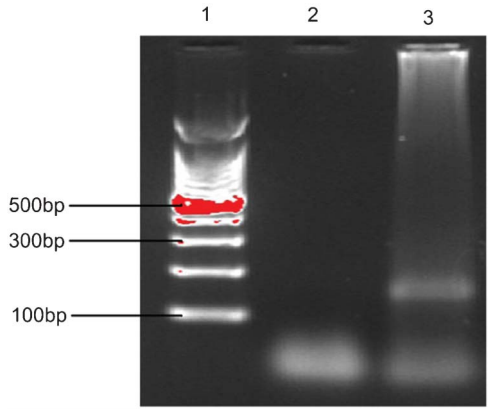

Fig. 9 Gel-like image of the end-point products following chip amplification after 30 min. Lane 1, lane 2 and lane 3 represent the DNA ladder, negative control (free of DNA template) and positive control reaction, respectively.

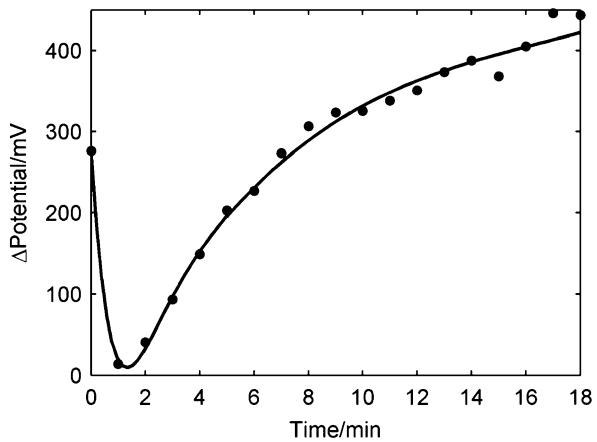

Fig. 10 Voltammograms show the NSDA reaction with 30 mM of trehalose. The chamber was incubated with 0.5% BSA for 60 min before the reaction. The measurement was executed at 35 kHz and 10 V.

The main advantage of this system is that the electrodes and the sample solution are completely isolated from each other, thereby avoiding electrode corrosion. If not physically damaged, there will be no loss of activity for the sensor, thereby making the microchips reusable for longer. Based on the studies described above, this C^4D system is capable of gaining a detection limit of lower than 2.5 μM for NSDA. Moreover, it takes the C^4D system only 7 min to finish amplification and EC detection. Several factors are essential to the excellent performance of the device: the structure of the IDEs, the insulation materials, and the signal processing methods. The IDEs cooperate with the insulation to determine the sensitivity and the resolution of the microchip. It is recommended that thinner insulation may be achieved using such materials as silicon carbide,[33] while rising graphene materials[34] are also considered to substitute for gold electrodes. By solving such key problems, the time cost in implementing the tasks of DNA amplification at lower initial concentrations and measurement can be limited to less than 5 min. It is impossible to quantify the starting template concentrations of NSDA, unless a NSDA calibration curve is produced by DNA amplification at different initial concentrations.

By directly measuring the conductivity of the amplification products, the contactless method has potential to distinguish single-stranded DNA from double-stranded DNA, and long chains from short chains in the same way as contact methods do. It is should be noted that C^4D sensors monitor the overall ionic activity of all processes and all yields in the solution, but are unable to distinguish between different sequences of DNA fragments. Other research achievements could be used to provide selective specificity for this method, *e.g.* specific primers, DNA indicators, probes and other techniques. Further studies on the quantification measurements as well as specific detection will be required in the future.

Conclusion

Up to now, DNA has been widely described as an electrical conductor and the conductivity of DNA has been rarely used to detect amplification products directly. The present study represents an integrated system for the first time to monitor real-time isothermal DNA amplification *in situ* using contactless biosensors in the absence of probes, redox indicators or nanoparticles. The IDE sensors described herein reach a very low detection limit and a high resolution, which cover the sensitivity shortage of single-finger electrodes for the C^4D sensor. The insulating layers made of cover slips have a good dielectric constant in contrast to slide glasses and PDMS films, and require relatively simple processing. Despite its preliminary character, this study clearly indicates the ability of the integrated device to measure and monitor label-free DNA amplification in real time at an initial concentration of 2.5 μM on chip within 10 min. The contactless electrodes are neither contaminated nor corroded, thereby giving the chip a high reuse rate and long life. The isothermal DNA amplification simplifies the instrumentation of the controlling system, and the label-free model minimizes the interference of DNA amplification. Trehalose and chip pretreatment further enhance the reaction productivity and further increase the sensitivity of the microchip. The performance of the microchips will be greatly improved if thinner film coatings[25] are employed and further studies on this will be summarized in our next study. In summary, the C^4D system designed for real-time NSDA measurement can be highly integrated and achieve high throughput, portability and low cost. The system is highly desirable for application in sites of poor conditions and field applications. We hope our findings lead to further research in EC biochips and can be expanded to molecular biology, environmental science, food monitoring, disease diagnosis, gene analysis and other potential applications.

Acknowledgements

This work was supported by grants from the 973 Program of the Ministry of Science and Technology of China (No. 2012CB933303, 2011CB707505), the National Key Technology R&D Program (No.2012BAK08B05), Major National Science and Technology Projects (No. 2009ZX10004_505) and grants from the Science and Technology Commission of the Shanghai Municipality (Grant Nos. 1052nm06100, 11nm0505800, 11391901900, 11JC1414400).

References

1 X. T. Luo and I. M. Hsing, *Analyst*, 2009, **134**, 1957–1964.
2 N. Nakamura, K. Ito, M. Takahashi, K. Hashimoto, M. Kawamoto, M. Yamanaka, A. Taniguchi, N. Kamatani and N. Gemma, *Anal. Chem.*, 2007, **79**, 9484–9493.
3 Y. Xiao, A. A. Lubin, B. R. Baker, K. W. Plaxco and A. J. Heeger, *Proc. Natl. Acad. Sci. U. S. A.*, 2006, **103**, 16677–16680.
4 D. Ozkan, A. Erdem, P. Kara, K. Kerman, B. Meric, J. Hassmann and M. Ozsoz, *Anal. Chem.*, 2002, **74**, 5931–5936.
5 T. H. Fang, N. Ramalingam, D. Xian-Dui, T. S. Ngin, Z. Xianting, A. T. Lai Kuan, E. Y. Peng Huat and G. Hai-Qing, *Biosens. Bioelectron.*, 2009, **24**, 2131–2136.
6 K. Kerman, M. Kobayashi and E. Tamiya, *Meas. Sci. Technol.*, 2004, **15**, R1–R11.
7 M. Liu, C. Luo and H. Peng, *Talanta*, 2012, **88**, 216–221.
8 K. Goto, H. Horiuchi, H. Shinohara, K. Motegi, K. Hashimoto, S. Hongo, N. Gemma, N. Hayashimoto, T. Itoh and A. Takakura, *J. Microbiol. Methods*, 2007, **69**, 93–99.
9 M. Kobayashi, T. Kusakawa, M. Saito, S. Kaji, M. Oomura, S. Iwabuchi, Y. Morita, Q. Hasan and E. Tamiya, *Electrochem. Commun.*, 2004, **6**, 337–343.
10 G. Marrazza, G. Chiti, M. Mascini and M. Anichini, *Clin. Chem.*, 2000, **46**, 31–37.
11 T. Defe'ver, M. Druet, D. Evrard, D. Marchal and B. Limoges, *Anal. Chem.*, 2011, **83**, 1815–1821.
12 S. Hason, J. Dvorak, F. Jelen and V. Vetterl, *Talanta*, 2002, **56**, 905–913.
13 R. Y. Lai, E. T. Lagally, S. Lee, H. T. Soh, K. W. Plaxco and A. J. Heeger, *Proc. Natl. Acad. Sci. U. S. A.*, 2006, **103**, 4017–4021.
14 X. Luo, T. M. Lee and I. Hsing, *Anal. Chem.*, 2008, **80**, 7341–7346.
15 X. Liu, X. Qu, J. Dong, S. Ai and R. Han, *Biosens. Bioelectron.*, 2011, **26**, 3679–3682.
16 F. Davis, M. A. Hughes, A. R. Cossins and S. P. J. Higson, *Anal. Chem.*, 2007, **79**, 1153–1157.
17 W. R. Vandaveer, S. A. Pasas-Farmer, D. J. Fischer, C. N. Frankenfeld and S. M. Lunte, *Electrophoresis*, 2010, **25**, 3549.
18 N. G. Walter and G. Strunk, *Proc. Natl. Acad. Sci. U. S. A.*, 1994, **91**, 7937–7941.
19 A. Joneja and X. Huang, *Anal. Biochem.*, 2011, **414**, 58–69.
20 B. Arneth, *Anal. Biochem.*, 2009, **385**, 26–33.
21 J. Wang, G. Chen and A. Muck, *Anal. Chem.*, 2003, **75**, 4475–4479.
22 J. Tanyanyiwa, E. M. Abad-Villar, M. T. Fernández-Abedul, A. Costa-García, W. Hoffmann, A. E. Guber, D. Herrmann, A. Gerlach, N. Gottschlich and P. C. Hauser, *Analyst*, 2003, **128**, 1019–1022.
23 A. Bonanni, I. Fernandez-Cuesta, X. Borrise, F. Perez-Murano, S. Alegret and M. del Valle, *Microchim. Acta*, 2010, **170**, 275–281.
24 D. Berdat, A. Marin, F. Herrera and M. A. M. Gijs, *Sens. Actuators, B*, 2006, **118**, 53–59.
25 W. K. T. Coltro, R. S. Lima, T. P. Segato, E. Carrilho, D. P. de Jesus, C. L. do Lago and J. A. F. da Silva, *Anal. Methods*, 2012, **4**, 25–33.
26 B. Liu, Y. Zhang, D. Mayer, H. Krause, Q. Jin, J. Zhao and A. Offenhäusser, *Electrophoresis*, 2011, **32**, 699–704.
27 V. Tsouti, C. Boutopoulos, I. Zergioti and S. Chatzandroulis, *Biosens. Bioelectron.*, 2011, **27**, 1–11.
28 T. P. Segato, W. Coltro, A. Almeida, M. Piazetta, A. L. Gobbi, L. H. Mazo and E. Carrilho, *Electrophoresis*, 2010, **31**, 2526–2533.
29 J. Liu, J. Wang, Z. Chen, Y. Yu, X. Yang, X. Zhang, Z. Xu and C. Liu, *Lab Chip*, 2011, **11**, 969–973.
30 F. Laugere, R. M. Guijt, J. Bastemeijer, G. van der Steen, A. Berthold, E. Baltussen, P. Sarro, G. W. K. van Dedem, M. Vellekoop and A. Bossche, *Anal. Chem.*, 2003, **75**, 306–312.
31 Z. Chen, Q. Li, O. Li, X. Zhou, Y. Lan, Y. Wei and J. Mo, *Talanta*, 2007, **71**, 1944–1950.
32 T. Lee, M. C. Carles and I. M. Hsing, *Lab Chip*, 2003, **3**, 100–105.
33 R. M. Guijt, E. Baltussen, G. van der Steen, H. Frank, H. Billiet, T. Schalkhammer, F. Laugere, M. Vellekoop, A. Berthold, L. Sarro and G. van Dedem, *Electrophoresis*, 2001, **22**, 2537–2541.
34 L. Lin, Y. Liu, L. Tang and J. Li, *Analyst*, 2011, **136**, 4732–4737.